Research Papers

GREENSUSMATER

Greensusmater
Vol. 2, No. 2, 2025
https://doi.org/10.62755/greensusmater.2025.2.2.62-69

Check for updates

Niobium oxide electrode performance boosted by molybdenum doping and calcination for supercapacitor applications

Muhammad Ramadhan Al Mubarok[1] Rima Nurfitria[1] Rizky Aflaha[2] Eka Nurfani[1,3] Aditya Rianjanu[1,3]

[1] *Department of Materials Engineering, Faculty of Industrial Technology, Institut Teknologi Sumatera, Terusan Ryacudu, Way Hui, Jati Agung, Lampung Selatan, 35365 Indonesia*
[2] *Department of Physics, Faculty of Mathematics and Natural Sciences, Universitas Gadjah Mada, Sekip Utara, BLS 21, Yogyakarta 55281, Indonesia*
[3] *Center for Green and Sustainable Materials, Institut Teknologi Sumatera, Terusan Ryacudu, Way Hui, Jati Agung, Lampung 35365, Indonesia*

Corresponding author: eka.nurfani@mt.itera.ac.id (EN); aditya.rianjanu@mt.itera.ac.id (AR)

ARTICLE HISTORY: Received: November 07, 2025 | Revised: November 27, 2025 | Accepted: November 29, 2025

ABSTRACT

Niobium pentoxide (Nb_2O_5) is a promising pseudocapacitive material for supercapacitor applications due to its high theoretical capacitance and electrochemical stability. However, its practical performance is hindered by low electrical conductivity and limited ion transport kinetics. In this study, we report the enhancement of Nb_2O_5 electrode performance through molybdenum (Mo) doping and thermal calcination. Mo-doped Nb_2O_5 nanostructures were synthesized via a hydrothermal method followed by calcination at 500 °C. Scanning electron microscopy (SEM) and energy-dispersive X-ray spectroscopy (EDS) confirmed the formation of a rougher surface morphology and homogeneous Mo distribution in the doped sample. X-ray diffraction (XRD) analysis revealed a phase transition from a distorted orthorhombic structure in pristine Nb_2O_5 to a more crystalline pseudohexagonal phase in Mo-Nb_2O_5-500. Electrochemical measurements demonstrated significantly enhanced capacitive behavior, with Mo-Nb_2O_5-500 achieving a specific capacitance of 55.3 F g^{-1} at a scan rate of 5 mV s^{-1}, approximately five times higher than that of the undoped material. All electrodes exhibited stable cycling performance. These results highlight the synergistic effect of Mo doping and calcination in improving the electrochemical properties of Nb_2O_5, providing a viable strategy for the development of high-performance pseudocapacitor electrodes.

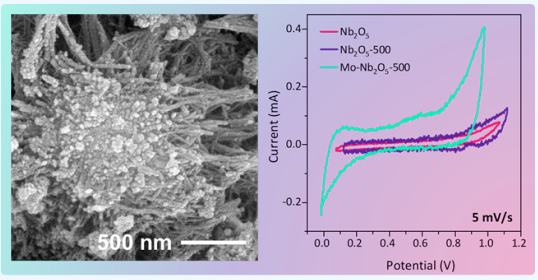

Keywords: *Niobium pentoxide (Nb_2O_5); Molybdenum doping; Calcination; Pseudocapacitor; Electrochemical performance*

1. INTRODUCTION

The rapid advancement of energy storage technologies has driven considerable interest in developing high-performance electrode materials for supercapacitors [1, 2]. Among various transition metal oxides, materials such as ruthenium dioxide (RuO_2) [3], manganese dioxide (MnO_2) [4, 5], cobalt oxide (Co_3O_4) [6, 7], and nickel oxide (NiO) [8, 9] have been extensively investigated for supercapacitor applications owing to their high specific capacitance and pseudocapacitive behavior. However, issues such as high cost (e.g., RuO_2), poor conductivity (e.g., MnO_2), or limited cycle life (e.g., NiO and Co_3O_4) constrain their practical application. In this context, niobium pentoxide (Nb_2O_5) has emerged as a promising candidate due to its high theoretical capacitance, wide electrochemical window, and excellent structural stability [10]. However, the practical application of Nb_2O_5 in supercapacitors remains limited by its inherently low electronic conductivity and relatively poor ionic diffusion kinetics, which result in suboptimal specific capacitance and rate performance [11].

To overcome these limitations, two principal strategies have been extensively explored: heteroatom doping and thermal treatment (calcination). Doping with transition metals such as molybdenum (Mo), tungsten (W), or vanadium (V) has been shown to effectively modulate the electronic structure of Nb_2O_5, introduce additional redox-active sites, and enhance electrical conductivity [12–14]. In particular, Mo doping can introduce donor states near the conduction band, facilitating faster electron transport and enabling pseudocapacitive charge storage through reversible faradaic reactions [15, 16]. Furthermore, doping may also influence the material's morphology and crystallinity, promoting more accessible surface area and optimized ion diffusion pathways.

Calcination, on the other hand, plays a critical role in improving the crystallinity and structural integrity of the synthesized Nb_2O_5. Controlled thermal treatment can reduce structural defects, enhance grain connectivity, and tune porosity, all of which contribute to improved electrochemical performance [17–19]. When combined with doping, calcination can synergistically reinforce the beneficial effects by stabilizing dopant distribution and promoting favorable microstructural evolution.

Despite previous efforts, the combined effect of Mo doping and calcination on the microstructure, elemental distribution, and electrochemical performance of Nb_2O_5 has not been fully elucidated. In this work, we synthesize Mo-doped Nb_2O_5 via a hydrothermal method followed by calcination and systematically investigate the impact of both modifications on the material's morphology, composition, and supercapacitor performance. The findings provide valuable

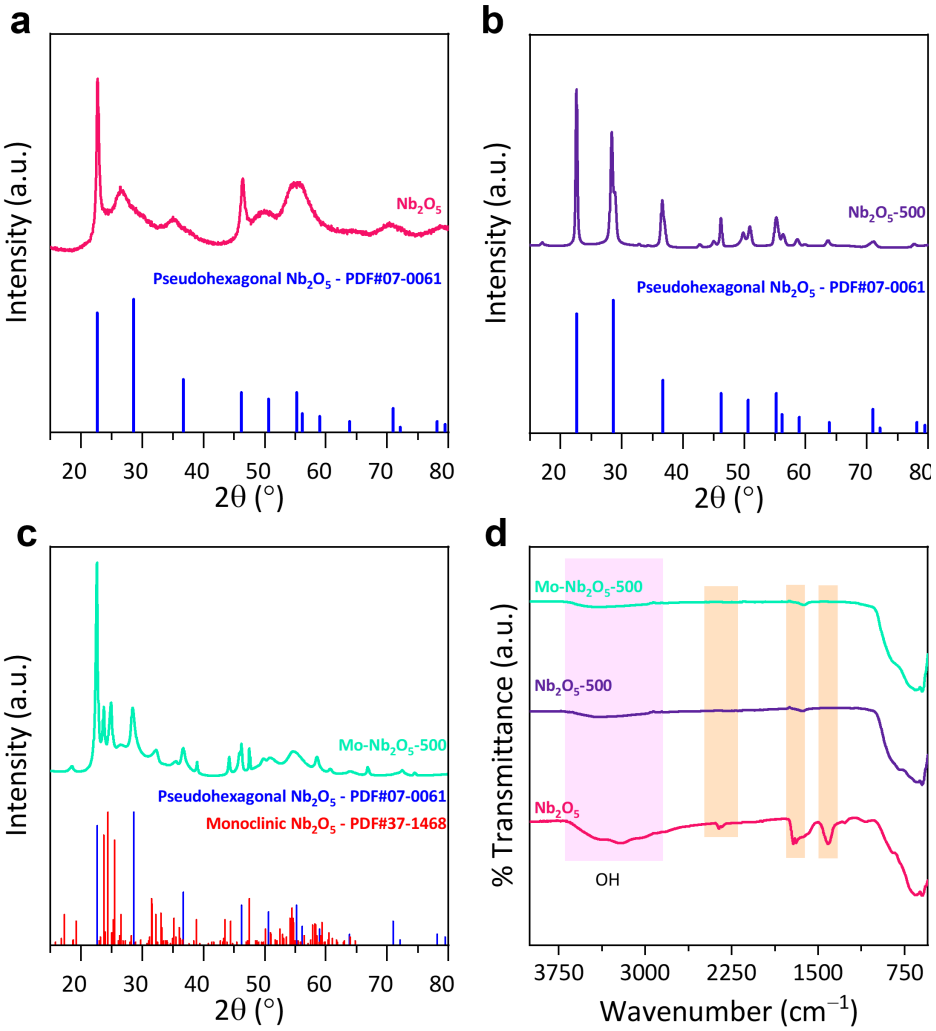

Figure 1. (a–c) X-ray diffraction (XRD) patterns of pristine Nb_2O_5, thermally treated Nb_2O_5 (Nb_2O_5-500), and Mo-doped Nb_2O_5 after calcination (Mo-Nb_2O_5-500), illustrating phase evolution and crystallinity changes; (d) Fourier-transform infrared (FTIR) spectra of the same samples, showing vibrational features and changes in bonding environment induced by calcination and Mo incorporation.

insights into the structure–property relationships in doped Nb-based oxides and offer a viable strategy for designing advanced electrode materials with enhanced capacitive behavior.

2. MATERIALS AND METHODS

2.1 Materials

High-purity ammonium niobate(V) oxalate hydrate (ANO, $C_4H_4NNbO_9 \cdot xH_2O$, 99.99% trace metals basis) and ammonium molybdate tetrahydrate (AMT, $(NH_4)_6Mo_7O_{24} \cdot 4H_2O$, 99.98% trace metals basis) were obtained from Sigma-Aldrich, Singapore. Deionized (DI) water was used as solvent during the hydrothermal process.

2.2 Preparation of Mo-Nb_2O_5 Nanoparticles

Mo-doped Nb_2O_5 nanostructures were synthesized via a hydrothermal method, adapted from previously reported studies [20]. In a typical synthesis, 3.4 g of ammonium niobate(V) oxalate hydrate were dissolved in 70 mL of DI water under continuous magnetic stirring at 600 rpm to ensure complete dissolution. Once a clear and homogeneous solution was obtained, 0.3 g of ammonium molybdate tetrahydrate was introduced as the molybdenum source. The resulting solution was transferred into a 100-mL Teflon-lined stainless-steel autoclave and subjected to hydrothermal treatment at 175 °C for 72 hours. Upon completion of the reaction, the precipitate was collected by vacuum filtration, thoroughly washed with deionized water to eliminate residual impurities, and dried in an oven at 80 °C for 6 hours. To improve crystallinity and electrochemical properties, the dried product underwent calcination in ambient air at 500 °C for 2 hours. This final sample was designated as Mo-Nb_2O_5-500. For comparative analysis, two control samples were also prepared: undoped Nb_2O_5 subjected to identical calcination conditions (Nb_2O_5-500), and uncalcined, undoped Nb_2O_5 (Nb_2O_5).

2.3 Materials Characterizations

The morphological and microstructural features of the synthesized samples were examined using scanning electron microscopy (SEM) performed on a JEOL JSM-6510 microscope equipped with an energy-dispersive X-ray spectroscopy (EDS) detector for elemental analysis and mapping. High-resolution

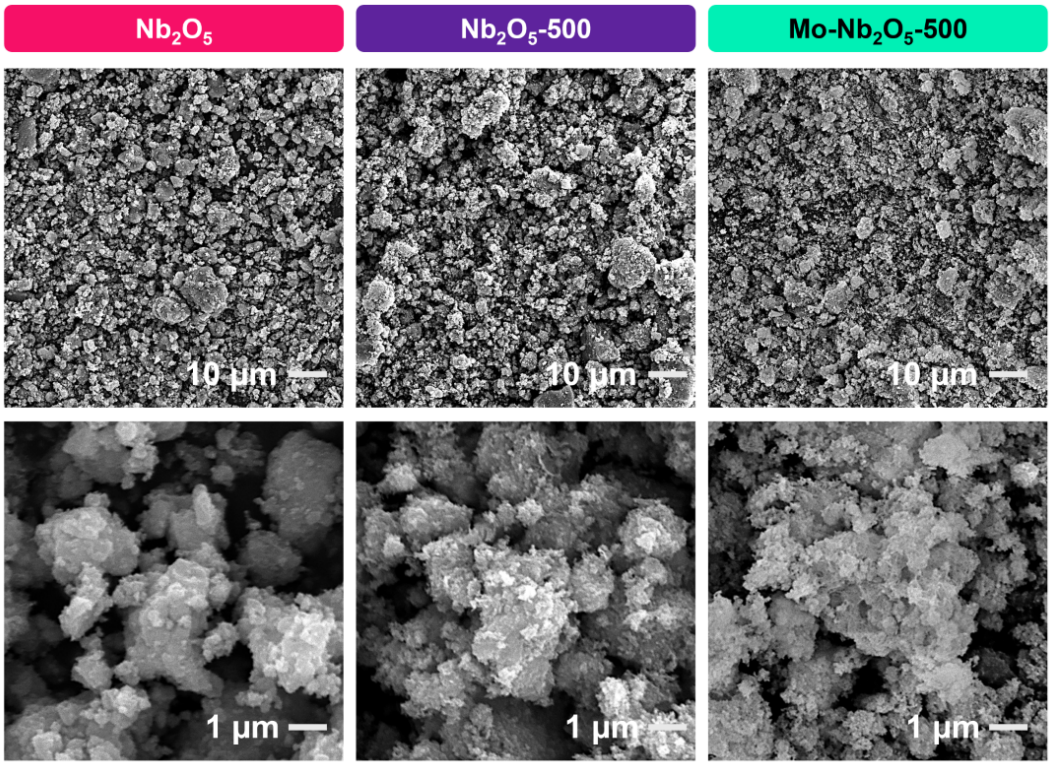

Figure 2. Scanning electron microscopy (SEM) images of Nb_2O_5, Nb_2O_5-500, and Mo-Nb_2O_5-500 samples at low (top row, 10 μm) and high (bottom row, 1 μm) magnifications, illustrating morphological evolution induced by thermal calcination and Mo doping. Notable changes include surface coarsening, increased particle definition, and textural roughening in the doped and calcined samples.

surface imaging was further conducted using field-emission scanning electron microscopy (FESEM) on a JEOL JSM-7610F to assess the finer details of particle morphology and surface texture. Phase composition and crystallographic structure were analyzed using X-ray diffraction (XRD) measurements carried out on a Rigaku SmartLab SE Basic diffractometer equipped with a Cu Kα radiation source (λ = 1.5406 Å). The XRD patterns were recorded over an appropriate 2θ range to identify phase purity and assess the effect of calcination and Mo doping on the crystal structure of the Nb_2O_5-based materials.

2.4 Electrochemical Investigation

Cyclic voltammetry (CV) measurements were conducted to evaluate the electrochemical performance of Nb_2O_5, Nb_2O_5-500, and Mo-Nb_2O_5-500 electrodes. The electrode slurry was prepared by mixing each active material (0.038 g) with PVDF binder (0.0127 g) and acetylene black (0.0127 g), followed by gradual addition of N-methyl-2-pyrrolidone (76 μL total, approximately 10 drops). The mixture was magnetically stirred for 1.5 h to obtain a homogeneous dispersion. Subsequently, 3 μL of slurry was drop-cast onto a glassy carbon electrode (GCE) and dried at 60 °C for 30 minutes to form the working electrode. CV tests were performed in 1 M Na_2SO_4 electrolyte using a three-electrode configuration: GCE as the working electrode, Ag/AgCl as the reference electrode, and Pt wire as the counter electrode. The measurements were carried out using a XPOW-AX-PST Potentiostat (Nicslab, Indonesia), and the obtained voltammograms were used to derive the effective specific capacitance of each sample [21, 22].

3. RESULTS AND DISCUSSION

The crystalline structures of Nb_2O_5, Nb_2O_5-500, and Mo-Nb_2O_5-500 were analyzed using X-ray diffraction (XRD), with the results presented in Figure 1a–c. The uncalcined Nb_2O_5 sample (Figure 1a) displays broad and relatively low-intensity peaks that resemble a deformed orthorhombic structure, indicative of poor crystallinity and potential structural disorder typically associated with as-synthesized Nb_2O_5 from hydrothermal methods [23, 24]. Such features suggest partial amorphization or the presence of nanocrystalline domains with local lattice distortions. Upon calcination, the XRD pattern of the Nb_2O_5-500 sample (Figure 1b) reveals significantly sharpened and more intense peaks that match well with the pseudohexagonal Nb_2O_5 phase (PDF#07-0061) [25, 26]. This suggests a substantial improvement in crystallinity, driven by thermal energy promoting atomic rearrangement and long-range structural ordering. The emergence of well-resolved peaks confirms that the calcination process effectively transforms the initially disordered structure into a more ordered crystalline phase.

Further enhancement is observed in the Mo-doped and calcined sample (Figure 1c). Mo-Nb_2O_5-500 displays even sharper peaks, consistent with the pseudohexagonal Nb_2O_5 phase and no secondary phases such as MoO_3, indicating successful Mo incorporation into the Nb_2O_5 lattice without inducing phase segregation. Additionally, minor features corresponding to the monoclinic phase (PDF#37-1468) are discernible [27, 28], suggesting a possible coexistence or intermediate phase during lattice reorganization. The preserved pseudohexagonal structure and improved crystallinity are

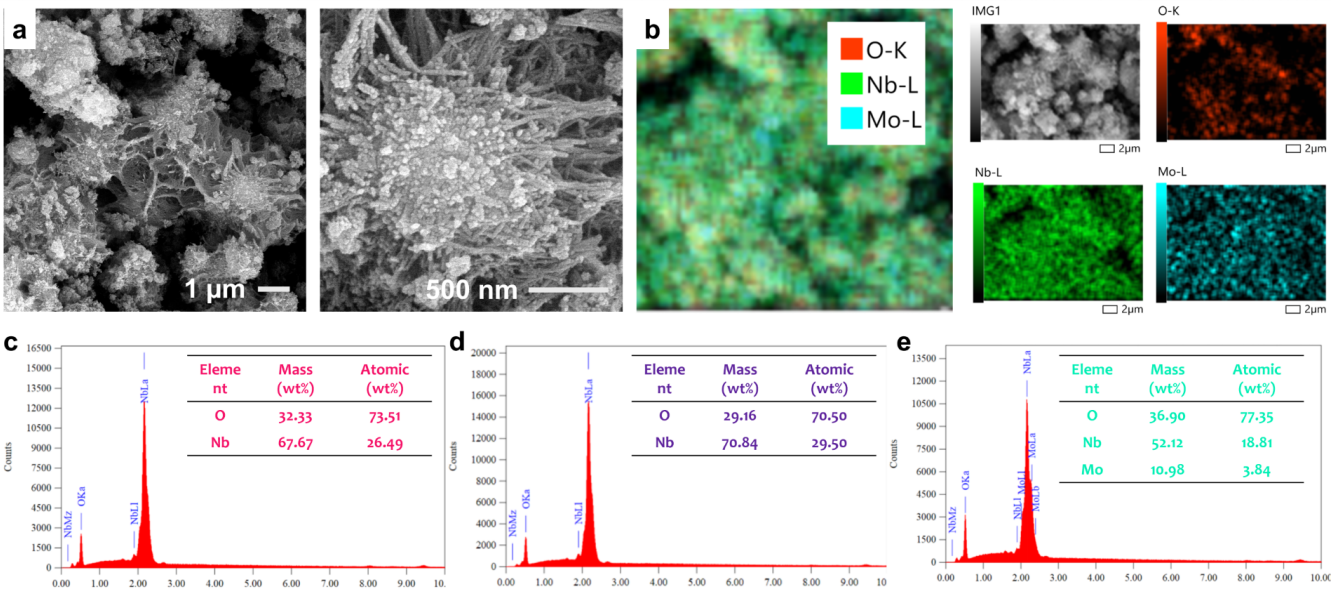

Figure 3. (a) Field emission scanning electron microscopy (FESEM) image showing the microstructure of Mo-Nb_2O_5-500; (b) energy-dispersive X-ray spectroscopy (EDS) elemental mapping confirming the uniform spatial distribution of oxygen (O), niobium (Nb), and molybdenum (Mo); (c–e) EDS spectra and corresponding elemental compositions for Nb_2O_5, Nb_2O_5-500, and Mo-Nb_2O_5-500, respectively, illustrating compositional evolution through calcination and Mo doping.

likely facilitated by both Mo doping and calcination. The close ionic radii of Mo^{6+} and Nb^{5+} support lattice substitution without significant distortion [16]. Previous studies have demonstrated that the incorporation of Mo atoms into the Nb_2O_5 lattice induces changes in lattice parameters, primarily attributed to an increase in interplanar (d) spacing [16]. Overall, the transition from a broad, amorphous-like pattern in Nb_2O_5 to well-defined crystalline features in Mo-Nb_2O_5-500 confirms the critical roles of both calcination and doping. The structural evolution toward a highly ordered pseudo-hexagonal phase is expected to enhance electron mobility, ion diffusion, and ultimately, electrochemical performance.

The Fourier-transform infrared (FTIR) spectra of Nb_2O_5, Nb_2O_5-500, and Mo-Nb_2O_5-500 (Figure 1d) are dominated by bands in the 900–500 cm^{-1} region, which are assigned to Nb–O stretching and Nb–O–Nb bridging vibrations of NbO_6 octahedra, characteristic of Nb_2O_5-based oxides. The overall shape and positions of these Nb–O-related bands are very similar for all three samples, indicating that neither calcination nor Mo doping alters the primary Nb_2O_5 framework. This is consistent with previous Mo-doped Nb_2O_5 work, where doping did not introduce new vibrational features but preserved the Nb_2O_5 lattice [16]. A broad absorption band between 3750 and 3000 cm^{-1} is observed for the as-prepared Nb_2O_5, associated with OH stretching of surface hydroxyl groups and adsorbed water, accompanied by a weaker band near 1630 cm^{-1} from H–O–H bending. Both features are markedly reduced in Nb_2O_5-500 and Mo-Nb_2O_5-500, confirming that calcination at 500 °C effectively removes most physisorbed water and a significant fraction of surface –OH species [29]. In the uncalcined Nb_2O_5, a weak band in the 1400–1500 cm^{-1} region can be ascribed to C=O vibrations from residual oxalate/organic precursor species, in agreement with previous Mo-Nb_2O_5 reports [16]; this band disappears completely in Nb_2O_5-500 and Mo-Nb_2O_5-500, confirming almost complete elimination of these residues after heat treatment [30]. Importantly, no new bands attributable to distinct Mo–O vibrations are observed for Mo-Nb_2O_5-500, and the positions of the Nb–O-related bands remain essentially unchanged, supporting that Mo is incorporated into the Nb_2O_5 lattice without forming separate MoO_x phases and without disrupting the Nb–O framework.

The surface morphologies of Nb_2O_5, Nb_2O_5-500, and Mo-Nb_2O_5-500 samples were examined using scanning electron microscopy (SEM), as presented in Figure 2. All samples exhibit aggregated nanoparticulate structures, with no distinct long-range ordering, indicating that the hydrothermal synthesis route yields similar granular morphologies regardless of post-treatment or doping. Upon calcination at 500 °C, the Nb_2O_5-500 sample shows a slightly more compact and fused particle arrangement compared to the uncalcined Nb_2O_5, suggesting enhanced grain connectivity due to thermal sintering. Interestingly, the Mo-Nb_2O_5-500 sample displays a surface morphology that remains largely similar to the calcined undoped counterpart but exhibits a visibly rougher texture and more irregular particle boundaries [31, 32].

The microstructure and elemental composition of the Mo-Nb_2O_5-500 sample were investigated using field-emission scanning electron microscopy coupled with energy-dispersive X-ray spectroscopy (FESEM-EDS), as presented in Figure 3. The SEM images (Figure 3a) reveal a rough, porous morphology composed of aggregated nanoparticles interspersed with thin, rod-like features [33]. This hierarchical structure likely results from anisotropic crystal growth facilitated by Mo incorporation during hydrothermal synthesis, followed by morphological restructuring during calcination. Such a morphology is advantageous for supercapacitor applications, as it offers a high surface area and promotes efficient electrolyte penetration and ion diffusion. To examine the spatial distribution of the constituent elements, EDS elemental mapping was performed (Figure 3b). The uniform distribution of oxygen (O), niobium (Nb), and molybdenum (Mo) signals confirms the successful and homogeneous doping of Mo into the Nb_2O_5 framework, with no evidence of phase

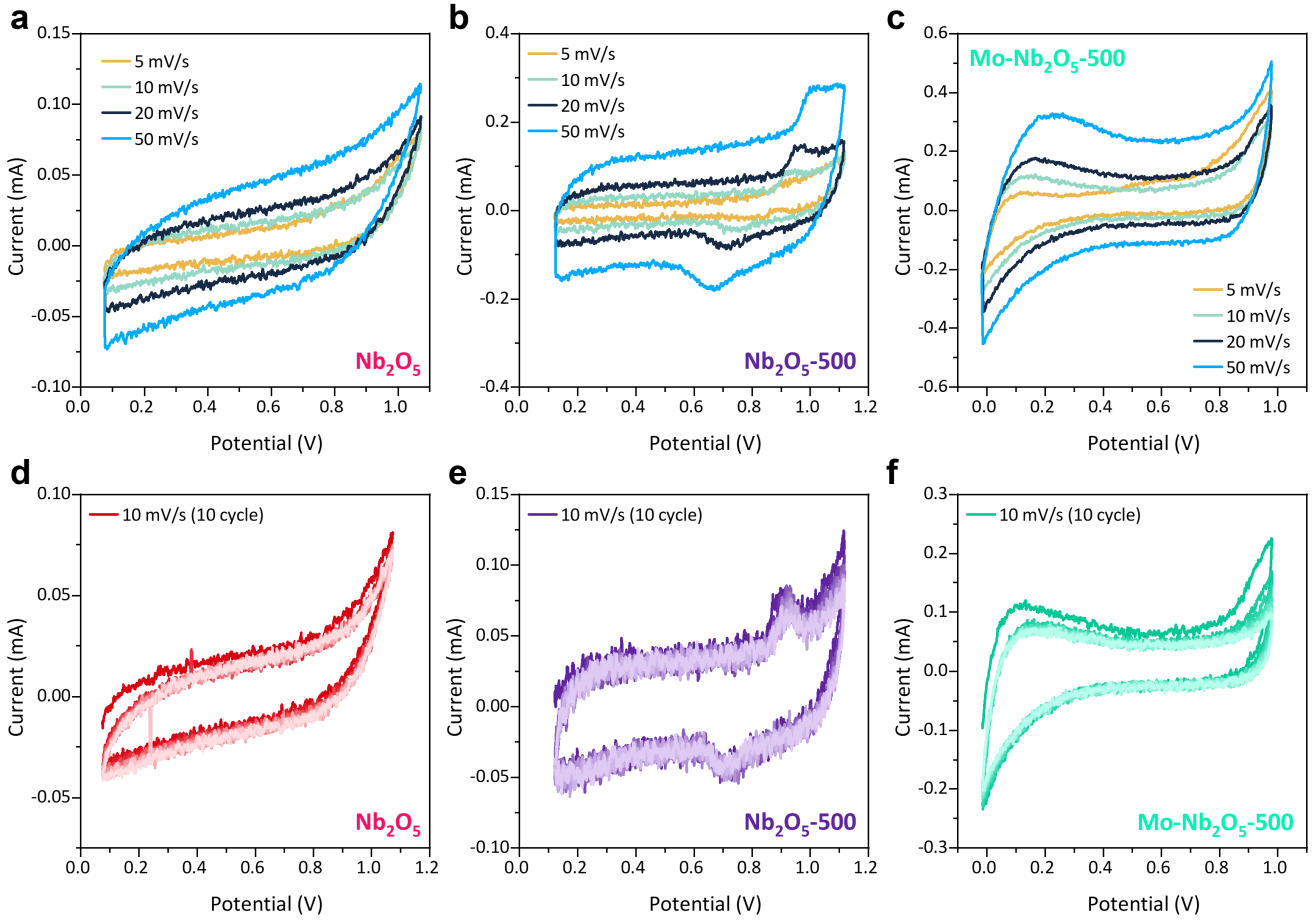

Figure 4. Cyclic voltammetry (CV) curves of (a) Nb_2O_5, (b) Nb_2O_5-500, and (c) Mo-Nb_2O_5-500 recorded at various scan rates, demonstrating capacitive behavior and rate responsiveness; (d–f) cycling stability profiles of the respective electrodes evaluated at a scan rate of 10 mV s^{-1} over 10 cycles, illustrating electrochemical durability and retention performance following calcination and Mo doping.

segregation or clustering. This uniformity is critical for ensuring consistent electronic properties throughout the material and maintaining structural integrity during electrochemical cycling.

The corresponding EDS spectra and quantitative analysis (Figures 3c–e) further validate the compositional differences among the samples. Both Nb_2O_5 and Nb_2O_5-500 show only Nb and O peaks, with stoichiometries close to the theoretical ratio, although slight shifts in O:Nb ratios are observed after calcination, likely due to structural densification and the removal of surface-bound species. In contrast, Mo-Nb_2O_5-500 exhibits a clear Mo peak, with a measured atomic concentration of 3.84%, confirming successful doping. The concurrent reduction in Nb atomic percentage suggests partial substitution or lattice incorporation of Mo, which can modulate the electronic structure and enhance redox activity.

The cyclic voltammetry (CV) curves of Nb_2O_5, Nb_2O_5-500, and Mo-Nb_2O_5-500 measured at various scan rates (5–50 mV/s) are presented in Figures 4a–c. Each sample demonstrates markedly different capacitive behavior. The CV curves of pristine Nb_2O_5 (Figure 4a) exhibit a near-rectangular shape with relatively low current response, indicative of electric double-layer capacitance (EDLC)-dominated behavior with limited faradaic contribution, likely due to its poor electronic conductivity and lack of active redox sites [34, 35]. In contrast, the calcined Nb_2O_5-500 sample (Figure 4b) displays a more distorted CV profile with broader humps, suggesting a transition from purely EDLC to a pseudocapacitive mechanism, likely enabled by enhanced crystallinity and increased surface redox activity due to thermal treatment. The current response is also notably higher than that of uncalcined Nb_2O_5, supporting the positive effect of calcination on electrochemical performance [36].

Mo-Nb_2O_5-500 (Figure 4c) exhibits the most pronounced pseudocapacitive behavior, as evidenced by its strong redox peaks and the highest current response among the three. This indicates that molybdenum doping introduces additional redox-active sites and facilitates improved charge storage kinetics, likely due to enhanced electrical conductivity and modified electronic structure [37]. The combination of Mo incorporation and calcination synergistically contributes to the improved capacitive behavior, making Mo-Nb_2O_5-500 a promising candidate for high-performance supercapacitor electrodes. The cycling stability of Nb_2O_5, Nb_2O_5-500, and Mo-Nb_2O_5-500 was further assessed over 10 consecutive CV cycles at 10 mV/s, as depicted in Figures 4d, e, and f, respectively. All three samples demonstrate excellent electrochemical reversibility, with minimal distortion and consistent CV profiles across multiple cycles. The near overlap of the CV curves suggests good structural integrity and stable charge–

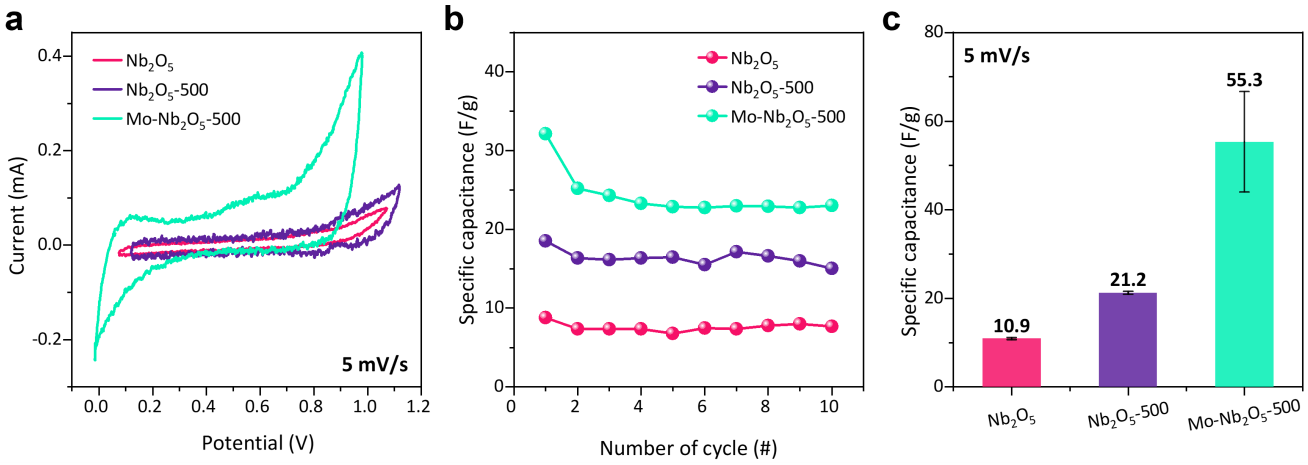

Figure 5. (a) Cyclic voltammetry (CV) comparison of Nb_2O_5, Nb_2O_5-500, and Mo-Nb_2O_5-500 electrodes at a scan rate of 5 mV s^{-1}, highlighting the enhanced capacitive response of the doped and calcined sample; (b) specific capacitance evolution over 10 cycles at 10 mV s^{-1}, indicating cycling stability; (c) bar chart of specific capacitance at 5 mV s^{-1}, showing a pronounced increase for Mo-Nb_2O_5-500 relative to the other samples.

discharge behavior, even for the uncalcined Nb_2O_5 sample. This indicates that the synthesized materials possess inherent robustness under repeated electrochemical operation.

The electrochemical performance of the three electrodes was directly compared through cyclic voltammetry (CV) and specific capacitance evaluation, as shown in Figure 5. The CV curves measured at 5 mV/s (Figure 5a) clearly show differences in capacitive behavior among the samples. Pristine Nb_2O_5 exhibits the lowest current response and the smallest CV area, indicating poor charge storage performance, which is consistent with its low crystallinity and absence of dopants. The calcined Nb_2O_5-500 electrode shows moderate improvement in current density and CV area, reflecting enhanced ion diffusion and conductivity resulting from improved crystallinity after thermal treatment. The Mo-Nb_2O_5-500 sample demonstrates a markedly larger CV area and more pronounced redox features, highlighting dominant pseudocapacitive behavior. This enhancement is attributed to the synergistic effect of Mo doping and calcination, which together improve surface reactivity, increase the number of redox-active sites, and enhance electron transport within the Nb_2O_5 framework.

To evaluate the cycling performance of each electrode, the specific capacitance over 10 consecutive CV cycles at 10 mV/s was monitored (Figure 5b). All samples exhibit stable cycling behavior with minimal capacitance loss, indicating good electrochemical reversibility. Notably, Mo-Nb_2O_5-500 retains the highest and most consistent capacitance across cycles, underscoring its superior structural and electrochemical stability [38]. The specific capacitance values calculated from CV curves at 5 mV/s are summarized in Figure 5c. The pristine Nb_2O_5 electrode delivers a specific capacitance of 10.9 F/g, which increases to 21.2 F/g after calcination. The Mo-doped and calcined sample achieves a significantly enhanced value of 55.3 F/g, confirming the effectiveness of combined doping and thermal treatment in enhancing charge storage capacity. These findings reinforce that Mo-Nb_2O_5-500 is the most promising candidate among the tested materials for high-performance supercapacitor electrodes.

4. CONCLUSION

In this study, we successfully synthesized Mo-doped Nb_2O_5 nanostructures via a hydrothermal method followed by calcination and systematically investigated their structural and electrochemical properties for supercapacitor applications. Scanning electron microscopy revealed that all samples maintained a similar aggregated morphology, with the Mo-doped and calcined sample (Mo-Nb_2O_5-500) exhibiting a rougher and more porous surface, which is favorable for ion accessibility. Elemental mapping and EDS analysis confirmed the homogeneous incorporation of Mo into the Nb_2O_5 matrix without forming secondary phases. X-ray diffraction analysis showed that the pristine Nb_2O_5 exhibited features of a deformed orthorhombic structure, while the Mo-Nb_2O_5-500 sample displayed a pseudohexagonal phase with enhanced crystallinity due to calcination. This structural improvement is associated with better charge transport pathways. Electrochemical measurements demonstrated that both calcination and Mo doping significantly enhanced the capacitive performance of Nb_2O_5. The Mo-Nb_2O_5-500 electrode achieved a specific capacitance of 55.3 F/g at 5 mV/s, substantially outperforming pristine Nb_2O_5 (10.9 F/g) and calcined Nb_2O_5 (21.2 F/g). All samples also exhibited stable cycling behavior, with Mo-Nb_2O_5-500 maintaining high capacitance and excellent reversibility over repeated cycles. Overall, the synergistic effect of Mo doping and calcination offers an effective strategy to enhance the electrochemical performance of Nb_2O_5-based electrodes, providing valuable insights for the design of advanced pseudocapacitive materials.

DATA AVAILABILITY STATEMENT

The datasets generated during and/or analyzed during the current study are available from the corresponding author on reasonable request.

CONFLICT OF INTEREST

The authors declare that there are no conflicts of interest associated with this publication, and there has been no significant financial support for this work that could have influenced its outcome.

REFERENCES

[1] F. Wang, X. Wu, X. Yuan, Z. Liu, Y. Zhang, L. Fu, Y. Zhu, Q. Zhou, Y. Wu, W. Huang, Latest advances in supercapacitors: from new electrode materials to novel device designs, Chemical Society Reviews 46 (2017) 6816–6854. https://doi.org/10.1039/C7CS00205J.

[2] Z. Yu, L. Tetard, L. Zhai, J. Thomas, Supercapacitor electrode materials: nanostructures from 0 to 3 dimensions, Energy & Environmental Science 8 (2015) 702–730. https://doi.org/10.1039/C4EE03229B.

[3] F. Yu, L. Pang, H.-X. Wang, Preparation of mulberry-like ruo_2 electrode material for supercapacitors, Rare Metals 40 (2021) 440–447. https://doi.org/10.1007/s12598-020-01561-8.

[4] E. Nurfani, P. Fau, N. I. Khamidy, R. Marlina, Effect of hydrothermal temperature on the structural and electrochemical properties of mno_2-based supercapacitors, Journal of Materials Science: Materials in Electronics 35 (2024) 2046. https://doi.org/10.1007/s10854-024-13820-w.

[5] P. Fau, L. M. Mahardhika, N. I. Khamidy, M. G. I. G. I. Khan, B. P. Prasetya, R. Y. Arundina, R. Marlina, E. Nurfani, The role of sintering temperature in mno_2 nanorods for supercapacitor applications: Phase evolution and enhanced capacitance, ECS Journal of Solid State Science and Technology (2025). https://doi.org/10.1149/2162-8777/ae1b6f.

[6] C. Lu, L. Liu, Y. Yang, Y. Ma, Q. Luo, M. Zhu, Recent progress in co_3o_4-based nanomaterials for supercapacitors, ChemNanoMat 9 (2023). https://doi.org/10.1002/cnma.202200537.

[7] S. Aslam, S. M. Ramay, A. Mahmood, G. M. Mustafa, S. Zawar, S. Atiq, Electrochemical performance of transition metal doped co_3o_4 as electrode material for supercapacitor applications, Journal of Sol–Gel Science and Technology 105 (2023) 360–369. https://doi.org/10.1007/s10971-022-06008-3.

[8] J. Wang, F. Zheng, M. Li, D. Jia, X. Mao, J. Fu, P. Hu, Q. Zhen, Y. Yu, Facile preparation of porous single crystal nio nanoflake array directly grown on nickel foam for supercapacitive electrode material, Journal of Alloys and Compounds 913 (2022) 165280. https://doi.org/10.1016/j.jallcom.2022.165280.

[9] T. Munawar, M. S. Nadeem, F. Mukhtar, S. Manzoor, M. N. Ashiq, F. Iqbal, Surfactant-assisted facile synthesis of petal-nanoparticle interconnected nanoflower-like nio nanostructure for supercapacitor electrode material, Materials Science and Engineering: B 284 (2022) 115900. https://doi.org/10.1016/j.mseb.2022.115900.

[10] R. Pang, Z. Wang, J. Li, K. Chen, Polymorphs of nb_2o_5 compound and their electrical energy storage applications, Materials 16 (2023) 6956. https://doi.org/10.3390/ma16216956.

[11] F. Shen, Z. Sun, Q. He, J. Sun, R. B. Kaner, Y. Shao, Niobium pentoxide based materials for high rate rechargeable electrochemical energy storage, Materials Horizons 8 (2021) 1130–1152. https://doi.org/10.1039/D0MH01481H.

[12] L. She, D. Liu, Y. Zhao, L. Dong, Z. Wu, X. Xue, Y. Tian, W. Du, C. Zheng, S. He, M. Zhang, Y. Liu, J. Gan, C. Li, Y. Gao, F. Qi, X. Ren, Y. Jiang, Y. Yang, M. Gao, H. Pan, Advances on defect engineering of niobium pentoxide for electrochemical energy storage, Small (2025). https://doi.org/10.1002/smll.202410211.

[13] K. Su, H. Liu, Z. Gao, P. Fornasiero, F. Wang, Nb_2o_5-based photocatalysts, Advanced Science 8 (2021). https://doi.org/10.1002/advs.202003156.

[14] M. B. Beg, L. Ali, M. Altarawneh, Investigating niobium oxide-based materials: Synthesis, characterization, and applications in heterogeneous catalysis, Catalysis Reviews (2025) 1–90https://doi.org/10.1080/01614940.2025.2564083.

[15] R. M. J. Lemos, R. D. C. Balboni, C. M. Cholant, C. F. Azevedo, A. Pawlicka, A. Gündel, W. H. Flores, C. O. Avellaneda, Molybdenum doping effect on sol–gel nb_2o_5:li^+ thin films: Investigation of structural, optical and electrochromic properties, Materials Science in Semiconductor Processing 134 (2021) 105995. https://doi.org/10.1016/j.mssp.2021.105995.

[16] A. Rianjanu, S. A. Muhtar, C. Siburian, K. D. P. Marpaung, R. Aflaha, S. E. M. Putra, A. Afandi, K. Triyana, F. F. Abdi, T. Taher, H. S. Wasisto, Tailoring urchin-like nb_2o_5 nanostructures with molybdenum doping to enhance adsorption efficiency and selectivity toward cationic dyes in wastewater treatment, Advanced Engineering Materials 27 (2025). https://doi.org/10.1002/adem.202402287.

[17] E. Abreu, M. Z. Fidelis, M. E. Fuziki, R. M. Malikoski, M. C. Mastsubara, R. E. Imada, J. L. Diaz de Tuesta, H. T. Gomes, M. D. Anziliero, B. Baldykowski, D. T. Dias, G. G. Lenzi, Degradation of emerging contaminants: Effect of thermal treatment on nb_2o_5 as photocatalyst, Journal of Photochemistry and Photobiology A: Chemistry 419 (2021) 113484. https://doi.org/10.1016/j.jphotochem.2021.113484.

[18] X. Dong, H. Wang, J. Wang, Y. He, P. Yang, S. Wang, X. Chen, C. Yang, F. Lu, The effects of calcination on the electrochemical properties of manganese oxides, Nanoscale Advances 5 (2023) 5309–5321. https://doi.org/10.1039/D3NA00332A.

[19] X. Zhao, P. He, Q. Ruan, Y. Guo, X. Yan, X. Zhang, B. Liu, H. Chen, J. Fan, Enhanced electrochemical performance of $lini_{0.6}co_{0.2}mn_{0.2}o_2$ cathode for lithium ion batteries via a modified calcination process, Journal of Electroanalytical Chemistry 965 (2024) 118361. https://doi.org/10.1016/j.jelechem.2024.118361.

[20] T. Taher, P. Maharani, S. A. Muhtar, A. Munandar, A. N. Sidiq, A. Rianjanu, High surface area ortho-nb_2o_5 as bifunctional adsorbent and photocatalyst for efficient removal of tetracycline antibiotics from wastewater, Science and Technology Indonesia 10 (2025) 916–923. https://doi.org/10.26554/sti.2025.10.3.916-923.

[21] L. E. Helseth, Comparison of methods for finding the capacitance of a supercapacitor, Journal of Energy Storage 35 (2021) 102304. https://doi.org/10.1016/j.est.2021.102304.

[22] A. Shokry, A. M. Elshaer, J. El Nady, S. Ebrahim, M. Khalil, High energy density and specific capacity for supercapacitor based on electrochemical synthesized polyindole, Electrochimica Acta 423 (2022) 140614. https://doi.org/10.1016/j.electacta.2022.140614.

[23] T. Murayama, J. Chen, J. Hirata, K. Matsumoto, W. Ueda, Hydrothermal synthesis of octahedra-based layered niobium oxide and its catalytic activity as a solid acid, Catalysis Science & Technology 4 (2014) 4250–4257. https://doi.org/10.1039/C4CY00713A.

[24] T. Taher, A. Yoshida, A. Lesbani, I. Kurnia, G. Guan, A. Abudula, W. Ueda, Adsorptive removal and photocatalytic decomposition of cationic dyes on niobium oxide with deformed orthorhombic structure, Journal of Hazardous Materials 415 (2021) 125635. https://doi.org/10.1016/j.jhazmat.2021.125635.

[25] G. Chen, J. Chen, S. Zhao, G. He, T. S. Miller, Pseudohexagonal nb_2o_5 anodes for fast-charging potassium-ion batteries, ACS Applied Materials & Interfaces 15 (2023) 16664–16672. https://doi.org/10.1021/acsami.2c21490.

[26] A. Zambotti, G. C. Nkala, S. Dutta, S. H. Bhimineni, N. Leport, A. Laperruque, J. N. Weker, P. Sautet, L. Pilon, B. Dunn, Probing the effect of atomic and morphological arrangements in the pseudocapacitive properties of tt-nb_2o_5 nanostructures, Solid State Ionics 429 (2025) 116990. https://doi.org/10.1016/j.ssi.2025.116990.

[27] L. Kong, X. Cao, J. Wang, W. Qiao, L. Ling, D. Long, Revisiting li^+ intercalation into various crystalline phases of nb_2o_5 anchored on graphene sheets as pseudocapacitive electrodes, Journal of Power Sources 309 (2016) 42–49. https://doi.org/10.1016/j.jpowsour.2016.01.087.

[28] C. L. Ücker, V. Goetzke, F. C. Riemke, M. L. Vitale, L. R. Q. de Andrade, M. D. Á. de Andrade, E. C. Moreira, M. L. Moreira, C. W. Raubach, S. S. Cava, Multi-photonic behavior of nb_2o_5 and its correlation with synthetic methods, Journal of Materials Science 56 (2021) 7889–7905. https://doi.org/10.1007/s10853-021-05770-z.

[29] F. A. Qaraah, S. A. Mahyoub, M. E. Hafez, G. Xiu, Facile route for c–n/nb_2o_5 nanonet synthesis based on 2-methylimidazole for visible-light driven photocatalytic degradation of rhodamine

b, RSC Advances 9 (2019) 39561–39571. https://doi.org/10.1039/C9RA07505D.

[30] R. Rathnasamy, P. Thangasamy, V. Aravindhan, P. Sathyanarayanan, V. Alagan, Facile one-pot solvothermal-assisted synthesis of uniform sphere-like nb_2o_5 nanostructures for photocatalytic applications, Research on Chemical Intermediates 45 (2019) 3571–3584. https://doi.org/10.1007/s11164-019-03809-0.

[31] D. Shen, T. Lan, S. Gu, H. Luo, W. Yue, Y. Li, M. Wei, Novel sea urchin-like niobium pentoxide as an electron transport layer for efficient and stable perovskite solar cells, Crystal Growth and Design 25 (2025) 9433–9440. https://doi.org/10.1021/acs.cgd.5c01201.

[32] N. Mohite, M. Shinde, A. K. Gupta, Y. Waghadkar, S. W. Gosavi, K. C. Mohite, R. Chauhan, S. Rane, Facile synthesis of hollow urchin-like nb_2o_5 nanostructures and their performance in dye-sensitized solar cells, Journal of Solid State Electrochemistry 24 (2020) 273–281. https://doi.org/10.1007/s10008-019-04481-5.

[33] J. Chen, H. Wang, G. Huang, Z. Zhang, L. Han, W. Song, M. Li, Y. Zhang, Facile synthesis of urchin-like hierarchical nb_2o_5 nanospheres with enhanced visible light photocatalytic activity, Journal of Alloys and Compounds 728 (2017) 19–28. https://doi.org/10.1016/j.jallcom.2017.08.266.

[34] X. Meng, Z. Guan, J. Zhao, Z. Cai, S. Li, L. Bian, Y. Song, D. Guo, X. Liu, Lithium-pre-intercalated t-nb_2o_5/graphene composite promoting pseudocapacitive performance for ultralong lifespan capacitors, Chemical Engineering Journal 438 (2022) 135492. https://doi.org/10.1016/j.cej.2022.135492.

[35] L. O. Animasahun, B. A. Taleatu, S. A. Adewinbi, A. A. Alayyaf, S. K. Mosa, V. Maphiri, H. Kim, A. Y. Fasasi, Pseudocapacitive na-ion storage in binder-less, carbon additive-free nb_2o_{5-x} electrode synthesised via solvothermal-assisted electro-coating with enhanced areal capacitance and lowered impedance parameters, Journal of Physics and Chemistry of Solids 196 (2025) 112336. https://doi.org/10.1016/j.jpcs.2024.112336.

[36] N. Jabeen, A. Hussain, A. Malik, A. Q. Alkhedaide, Engineering of nb_2o_5-based composite for a dual theoretical and experimental study to investigate superior electrochemical performance, Materials Science in Semiconductor Processing 200 (2025) 109908. https://doi.org/10.1016/j.mssp.2025.109908.

[37] S.-J. Zhang, H. Chen, Y.-X. Xu, C.-S. An, K.-X. Xiang, Facile preparation of nb_2o_5 microspheres and their excellent electrochemical performance in aqueous zinc-ion hybrid supercapacitors, Rare Metals 41 (2022) 3129–3141. https://doi.org/10.1007/s12598-022-02016-y.

[38] J. Liu, K. Xiang, W. Zhou, Y. Zhu, L. Xiao, W. Chen, H. Chen, Preparation of nb_2o_5 with an air filter-like structure and its excellent electrochemical performance in supercapacitors, Journal of Alloys and Compounds 802 (2019) 668–674. https://doi.org/10.1016/j.jallcom.2019.06.191.

